Soft Matter

Accepted Manuscript

ROYAL SOCIETY OF CHEMISTRY

www.rsc.org/softmatter

Effects of particle softness on shear thickening of microgel suspensions

*Zhi Zhou,[1, 2] Javoris V. Hollingsworth,[1] Song Hong,[3] Guangmin Wei,[1] Yu Shi,[1] Xi Lu,[1] He Cheng,[4,] * Charles C. Han[1,]**

[1]State Key Laboratory of Polymer Physics and Chemistry, Joint Laboratory of Polymer Science and Materials, Beijing National Laboratory for Molecular Sciences, Institute of Chemistry, CAS, Beijing 100190, China

[2]University of Chinese Academy of Sciences, Beijing 100049, China

[3]Analysis and Test Centre, Beijing University of Chemical Technology, Beijing 10029, P. R. China

[4]China Spallation Neutron Source, Institute of High Energy Physics, Dongguan, Guangdong 523803, P. R. China

* To whom correspondence should be addressed.

Phone: 86-010-82618089. Fax: 86-010-62521519. E-mail: chenghe@iccas.ac.cn; c.c.han@iccas.ac.cn.

Abstract:

A series of microgel particles composed of a polystyrene (PS) core and thermo-sensitive poly (N-isopropylacrylamide) (PNIPAM) shell with different shell thicknesses were investigated to elucidate the effect of microgel softness on its shear thickening behavior. Since the softness of the microgels increases with decreasing temperature through the volume phase transition effect of PNIPAM shell, the measured softness parameter, n, which is derived from the Zwanzig-Mountain equation, was used to measure and describe the combined influences of temperature and shell thickness. Confocal microscopy is used to investigate the interaction potential between microgel particles with different softness parameters. According to the obtained results, the softness parameter can provide an estimate for the shear thickening behavior of microgel suspensions, at least semi-quantitatively.

1. Introduction

A concentrated colloidal suspension may exhibit shear thickening behavior as the applied shear rate is increased. Here, shear thickening refers to an abrupt increase in viscosity as a function of shear rates. This interesting feature is of great importance to many systems and has been exploited for applications ranging from soft armor to shock and energy absorption materials.[1–3]

Most of the previous studies in this field have focused on the shear thickening of hard sphere systems, such as silica,[4,5] poly (methyl acrylate) (PMMA) [6]and PS[7], with emphasis on the effects of particle size, polydispersity, and the shape of particles. However, very little attention has been given to soft microgel systems, which may be partly due to their difficulty to exhibit shear thickening behavior. Senff, Richtering and Ballauff[8–10] et al. examined the flow curves of soft microgel systems (e.g., pure PNIPAM microgels) and found no shear thickening behavior, even when it was near its volume phase transition temperature (VPTT). The noted differences between hard and soft sphere systems raise several important questions: Can shear thickening occur for soft microgel systems, and if so, what is the effect of softness on shear thickening? And what is the definition and boundary defining the "hard" vs. "soft"?

The softness of microgels particle can be calculated using the Zwanzig-Mountain equation, which relates the elastic modulus of isotropic materials to the interaction potential and pair correlation function.[11] Paulin et al.[12] modeled the interaction potential of concentrated microgel dispersions as a power law repulsion, yielding a scaling law behavior for the concentration dependence of the plateau modulus for

PMMA spheres. Senff and Richtering et al.[8,9] also used this relationship to indicate the softness of PNIPAM and PS-PNIPAM core-shell particles, and it fit the data well. Petekidis[13] distinguished the differences in softness for hard spheres, microgels and star-like micelles.

Inspired by the previously mentioned works, we used PS-core/PNIPAM-shell microgels (PS-N) with different shell thicknesses as a model system to evaluate the effect of particle softness on shear thickening. On one hand, soft microgels can have a much higher packing density than the random close packing limit of hard spheres because they can be deformed and packed to accommodate more particles within the same volume. On the other hand, shear thickening is supposedly strongly affected by the delicate balance between hydrodynamic interactions, Brownian motion and inter-particle interactions.[14] The volume phase transition of the PS-core/PNIPAM-shell microgel allows us to control and study the balance of these three parameters and possibly revealing the effect of microgel softness on shear thickening.

In this study, the core-shell particles are synthesized via a seeded emulsion polymerization process[15–18] at different PNIPAM/PS ratios. As a result, the softness can be changed in a single system by controlling the temperature and shell thickness. To observe the monodispersed spherical morphology of the core-shell microgels, transmission electron microscopy (TEM) is used. Next, temperature dependent dynamic light scattering (DLS) measurements are conducted to describe the conformation variation of the particles. The effective volume fractions of the particles

are then calibrated through the viscosity and hydrodynamic radius of the dilute suspensions. Finally, the softness of the particles is characterized with the Zwanzig and Mountain equation by rheological measurements. It was found that particle softness can be used as a semi-quantitative parameter to estimate the shear thickening behavior of PS-core/PNIPAM-shell microgel suspensions. Because this microgel system can be easily tuned, ranging from near hard spheres to soft microgels, it can be used as a suitable model to investigate the mechanism of shear thickening in detail.

2 Experimental Section

2.1 Materials

N-isopropylacrylamide (NIPAM, 97%, from Aldrich) was purified by recrystallization in hexane. Styrene (98%, from Sinopharm Chemical) was purified via passage through a basic alumina column to remove the inhibitor before use. Sodium dodecyl sulfate (SDS, 99%, from Beijing Chemical),

N, N'-methylenebisacrylamide (BIS, 99%, from Alfa Aesar), potassium peroxodisulfate (KPS, 99%, from Sigma-Aldrich), were used as received. Distilled deionized water, obtained from a Milli-Q water purification system (Millipore, Bedford, MA, USA), was used for the preparation of all aqueous solutions.

2.2 Synthesis of core-shell particles

Following the procedure of Kim and Ballauff[15], thermosensitive core-shell particles were synthesized by a seeded emulsion polymerization process described in the following sections.

2.2.1 Core latex

The emulsion polymerization was performed in a 500 mL three-necked flask equipped with a magnetic stirrer, reflux condenser and thermometer. Inside the flask, styrene (51.20 g), NIPAM (2.70 g), and SDS (0.48g) were dispersed in water (200mL). The mixture was heated to 80 ˚C in an argon atmosphere, and stirred at 400 rpm. KPS (0.60 g) was first dissolved in water (10 mL) and then added into the flask. After 8 hrs, the latex was dialyzed against water extensively for about 3 weeks.

2.2.2 Core-shell latex

In the second step, the PNIPAM shell was attached to the PS core. The prepared core latex (24.00g, solids content 17 wt %) was diluted with water (200 mL). Different amounts of NIPAM and BIS were then added at the same ratio; a detailed recipe is shown in Supporting Information. Three samples with different NIPAM/ PS ratios (PS-N 1, PS-N 2, and PS-N 3) were synthesized. The shell of PS-N 1 sample is the thinnest, and that of PS-N 3 sample is the thickest, as shown in Table 1. After the stirred mixture was heated to 80 ˚C, KPS (0.04 g dissolved in 10 mL water) was added to initiate the reaction. After 8 hrs, the reaction was stopped. The final core-shell latex was dialyzed against water and lyophilized to obtain the powder of the microgels.

2.3 Preparation of Suspension

Inside a vial, dried core-shell particles and water were added to form a suspension. To avoid water evaporation, the lid of the vial was sealed with parafilm. The suspension was then homogenized by ultrasonication for 10 min at about 28^{o}C. To fully swell the

PNIPAM, the vial was placed at room temperature.

2.4 Instrumentation

The TEM was operated at an acceleration voltage of 200kV with a JEOL-JEM 2100. All images were recorded digitally with a Gatan 832 CCD camera. Negative staining was performed by placing the sample grid on a drop of 1.5 wt. % phosphate-tungstic acid (PTA) aqueous solution for 5 min followed by air-drying.

Dynamic light scattering experiments were conducted using a commercial light scattering (LS) spectrometer equipped with a multi-τ digital time correlator (ALV5000). A cylindrical 22 mW UNIPHASE He-Ne laser (λ_o = 632.8 nm) was used as the light source. The spectrometer has a high coherence factor because of a quasi-single-mode fiber coupled with an efficient avalanche photodiode as the detector. The LS cell is held in a thermostated index matching vat filled with purified and dust free toluene, with temperature controlled to within 0.1^{o}C.

All rheological measurements were performed on a stress-controlled rheometer (Haake MARS III). A solvent trap is used around the sample to prevent solvent evaporation. Steady shear and oscillatory tests were all performed on 35 mm cone-plate geometry. Prior to each measurement, the sample was loaded at 30^{o}C and the temperature was then lowered to equilibrate for 10 minutes. The sample was presheared at a frequency of 1 rad/s and amplitude of 0.1 Pa for 10 minutes. Reproducible results are obtainalbe with this protocol.

2.5 Determination of effective volume fraction

Because the PNIPAM shell is swollen with water, the volume fraction of the

core-shell particles cannot be estimated directly by its weight fraction.[19] For a dilute suspension, the effective volume fraction, $\Phi_{eff,}$ can be determined from the relative viscosity, η/η_s, via an expression derived by Batchelor.[20]

$$\frac{\eta}{\eta_s} = 1 + 2.5\Phi_{eff} + 5.9\Phi_{eff}^2 \quad (1)$$

Here, η and η_s are the viscosities of the suspension and the solvent, respectively. The Φ_{eff} can be substituted by hc, where c is the weight fraction of the suspension and h is a shift factor for converting the weight fraction to effective volume fraction. In this study, the effective volume fractions of all samples were all calculated by $\Phi_{eff}=hc$.

Three distinct samples at three different temperatures were labeled and calibrated by DLS and TEM as shown in Table 1.

Table 1 Characterization of three samples at different temperatures

Samples	Weight Fraction of the Shell (wt %)	Temperature (^{o}C)	Converting Factor (h)	Hydrodynamic Radius (R_h) / nm
PS-N 1	20	30	1.56	57
PS-N 1	20	28	1.67	58
PS-N 1	20	25	2.76	61
PS-N 2	33	30	3.1	79
PS-N 2	33	28	3.7	83
PS-N 2	33	25	5.1	94
PS-N 3	50	30	4.7	92
PS-N 3	50	28	5.9	99
PS-N 3	50	25	6.8	104

3 Results and discussion

Particle softness is an important parameter, and its effect on shear thickening has been investigated by a few groups. For instance, Wagner et al. used a series of different hard sphere systems (i.e. silica and PMMA) to study the influence of particle softness on shear thickening behavior.[21] Petekidis et al. also compared the rheological behavior of different hard sphere and soft particle systems to determine the effects of particle softness.[13,22] Nevertheless, the effect of particle softness on shear thickening from different systems is still not clearly understood. Mewis et al. investigated the shear

thickening behavior of particles grafted or absorbed with polymer[23,24]. However, the presence of polymer on the particle surface can alter the lubrication force, which makes the system more complicated[25]. Therefore, in this study, a series of PS-N microgels with different shell thicknesses were used as a versatile model system to evaluate the role of particle softness on shear thickening. By controlling temperature and shell thickness, the softness can be adjusted in a single system.

3.1 Characterization of the microgel

Prior to performing the rheological measurements, the PS-N microgels were characterized by DLS and TEM. Figure 1 displays the volume phase transition (VPT) process of PS-N 1, PS-N 2 and PS-N 3; the inset shows their corresponding TEM images of dry particles. The original PS latex is 53±3 nm in radius by TEM, which is similar to its corresponding hydrodynamic radius (52 nm) in DLS, because it is a non-draining hard sphere in water. Due to the negative staining by PTA, the corona-like structure surrounding the spherical cores in the TEM images indicate the PS core/PNIPAM shell morphology. The images also show that the thickness of the PNIPAM shell increases from PS-N 1 to PS-N 3 with the increase of PNIPAM contents. The overall size of PS-N core-shell microgels in TEM is much smaller than that in DLS, due to its staining effect and the soft shell.

The VPT process of the microgels was shown in Figure 1. PNIPAM microgels are temperature-sensitive, and will release "bound water" when it is higher than its VPTT because of an entropy-dominated effect[26–29]. Therefore, the size and interaction of the microgel can be conveniently tuned by temperature. Figure 1(a) indicates that PS-N 1

has a lower VPTT near 28°C than homogeneous PNIPAM, and its hydrodynamic radius exhibits minimal changes during the volume phase transition process. This influence may be the result of the hydrophobic PS core, as it has been reported that the VPTT of PNIPAM decreases when linked with hydrophobic parts.[30] It should also be noted that due to the charge stabilization, the PS-N 1 samples do not flocculate at 28°C and 30°C.[31] In Figure 1(b) and 1(c), PS-N 2 has a slightly lower VPTT at 31°C and PS-N 3 has nearly the same VPTT (i.e., 32°C) as pure PNIPAM microgels. For PS-N 3, the hydrodynamic radius decreases from 110nm to 60nm during the volume phase transition, which enables us to change the softness and volume fraction of the microgel conveniently.

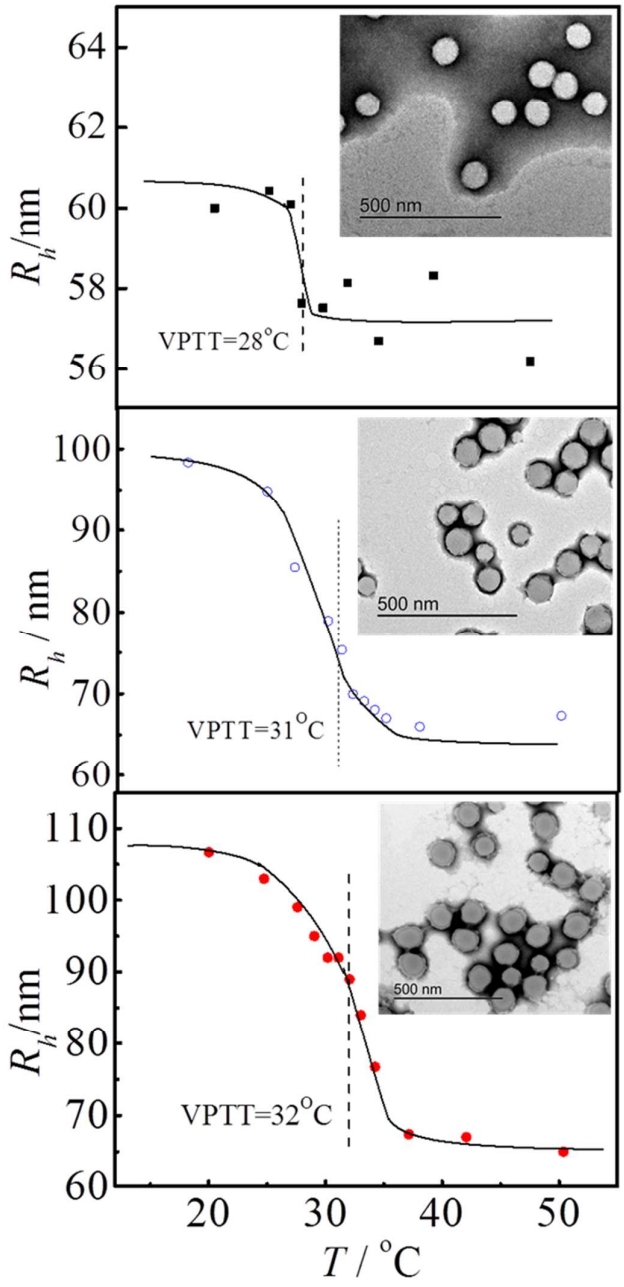

Figure 1.Hydrodynamic radius, R_h, as a function of temperature for microgels with different shell thickness: (a) PS-N 1; (b) PS-N 2; (c) PS-N 3. The lines are used to guide the eyes. The insets are the corresponding TEM images of dried particles with PTA negative staining. The inflection point is regarded as the VPTT.

3.2 Determination of particle softness

In this section, the softness of three different samples at three distinct temperatures (25°C, 28°C, and 30°C) is characterized. For PS-N 2 and 3, the three temperatures are all below its VPTT; whereas for PS-N 1, 28°C is near its VPTT and 30°C is above its VPTT, but lower than its binodal point These findings are in accordance with a study by Hu et al.[32], which reported the interaction potential of PNIPAM particles at different temperatures. Their phase diagram suggests that the overall interaction between microgels is repulsive below the binodal line. Also, it is known that the attraction between particles which stems from hydrophobic effects[33] arises across the VPTT. However, the negatively charged PNIPAM core-shell particles have an enhanced stability against flocculation, even above the VPTT (see Figure 1).[34] Moreover, PS-N 1 could not form the gel until 32°C (see Figure 1s in Supporting Information). Both of these observations indicate that the overall interaction of the PS-N 1 sample is still repulsive below 32°C

It has been reported that the softness of particles in suspension can be related to its elastic modulus can be measured using the following relationship derived from the Zwanzig and Mountain equation: [8,11,12,35]

$$G_p \propto \phi_{eff}^n \qquad (6)$$

This relation assumes the repulsive interaction potential of concentrated microgel dispersions is modeled as $U(r) \propto (\frac{1}{r})^m$. Accordingly, the *m* and *n* can be related via $n=1+m/3$. The simple interaction potential model was proposed to describe the interaction of poly (12-hydroxylstearic acid) (PHSA) stabilized PMMA particles[36]. It

was also used to represent the interactions in PNIPAM and PS core/PNIPAM shell microgels [8,9,13,37]. Since the overall interaction potentials in our PS-N microgel system are all repulsive below 32°C, eq. (6) should also be applicable. Here, the exponent *n* represents the softness parameter, which was used to determine the softness of the microgels. For ideal hard spheres, *n* should be infinity, while softness of microgels increases as *n* decreases. Of course, this is also reflected in the softer repulsive potential of *U(r)* as *n* decreases.

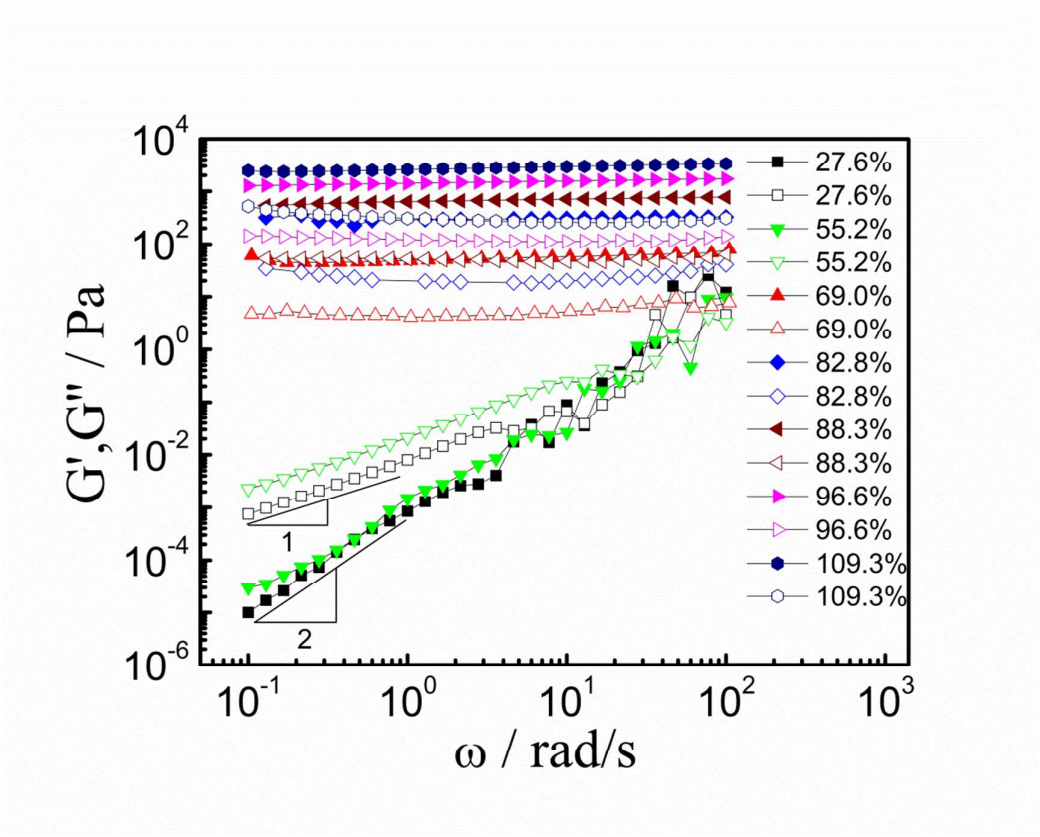

Figure 2. Frequency dependence of the storage modulus *G′* (filled symbols) and the loss modulus *G″* (open symbols) in PS-N 1 suspensions at various concentrations. The stress amplitude is 1 Pa for dense suspensions (concentration larger than 55.2%), and 0.1 Pa for dilute suspensions at a temperature of 25°C. The effective volume fraction

were calculated according to $\Phi_{eff}=hc$ and h from Table 1.

Figure 2 shows the oscillatory frequency sweep test of PS-N 1 at 25°C for various volume fractions. At high concentrations, the dispersions behave as a viscoelastic solid with the storage modulus G' higher than the loss modulus G'' in the whole frequency range. G' is nearly independent of frequency and corresponds to the plateau modulus G_p. While at low concentrations, the samples changed to a viscoelastic liquid with $G''>G'$, and power law relations, $G' \propto \omega^2, G'' \propto \omega$, are also found.[38] All samples were tested similarly.

Through the measurement of plateau modulus at different volume fractions, the softness parameter, n, can be obtained by a double logarithmic plot of G_p versus Φ_{eff}, as shown in Figure 3. In table 2, each of the fitting results are given. It can be clearly seen that the softness parameter of the particles increases dramatically with the decrease of shell thickness and increases with increasing temperature. For the "softest" PS-N 3 microgel at 25°C, n=5.0 is very close to that of pure PNIPAM microgels (n=4.2).[8] For the "hardest" PS-N 1 sample at 30°C, n=13.1 is close to that of model hard spheres[13]. Because of the existence of the soft and permeable PNIPAM shell, the system can only be close to but not exactly ideal hard sphere. Therefore, the softness is systematically changed from pure soft microgel to near hard sphere in one system simply by decreasing the shell thickness and increasing the temperature.

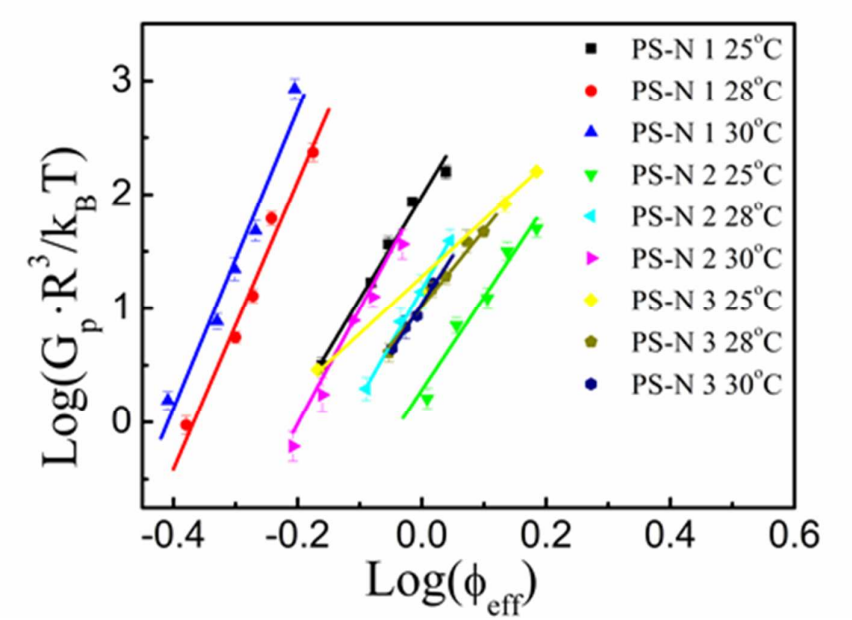

Figure 3. Plateau modulus scaled by the particle size and temperature versus the effective volume fraction for different samples at various temperatures. The lines represent the best fit according to Eq. (6).

Table 2. Softness parameter (*n*) of microgels at different temperatures

Temp. /°C	PS-N 1	PS-N 2	PS-N 3
25	9.1	8.3	5.0
28	12.6	9.6	6.7
30	13.1	10.2	8.5

3.2 Characterization of interaction potential between microgel particles

As previously discussed, the Zwanzig-Mountain equation linked the interaction between particles and their suspension rheology behavior. By comparing the rheology response of samples at different temperatures, the difference in particles softness and

interaction potential can be obtained. To study the exhibited effect of particle softness more directly, confocal microscopy was used to measure the interaction potential between particles[39].

The pairwise interaction potential between colloidal particles in a medium can be obtained from the equilibrium structure of particle suspensions[40,41]. In the system, the radial distribution function $g(r)$, which provided the possibility of finding neighboring particles at specific center-center distance, was calculated from the captured images of fluorescently labeled core-shell composites by averaging over 5000 particles. For dilute suspensions, $g(r)$ is directly associated to the interaction potential between particles $U(r)$ by balancing the Brownian and interparticle forces as $\lim_{\phi\to 0} g(r) = \exp[-\frac{U(r)}{k_B T}]$.

In the confocal microscopy experiments, dilute core-shell microgel suspensions were first mixed with hydrophobic dye, perylene. The imaging was then recorded using a Zeiss LSM 780 confocal microscope. At a temperature of 25°C, the interaction potential of PS-N 1 and PS-N 3 was measured. Here, the power law potential $U(r) \propto (\frac{1}{r})^m$ was also used to fit the data. As shown in Figure 4, in comparison to PS-N 1 at 25°C, the interaction potential of PS-N 3 decreases more slowly with center-to-center distance; therefore, the corresponding repulsive force of PS-N 3 is much larger than that of PS-N 1. This observation is consistent with the rheology results shown in Table 2, and confirms that PS-N 1 is much softer than PS-N 3 at 25°C. As particle softness increases from hard sphere to pure soft microgel by increasing the soft shell thickness, the interaction potential decreases more slowly

with center-to-center distance, while the repulsive force between particles becomes larger.

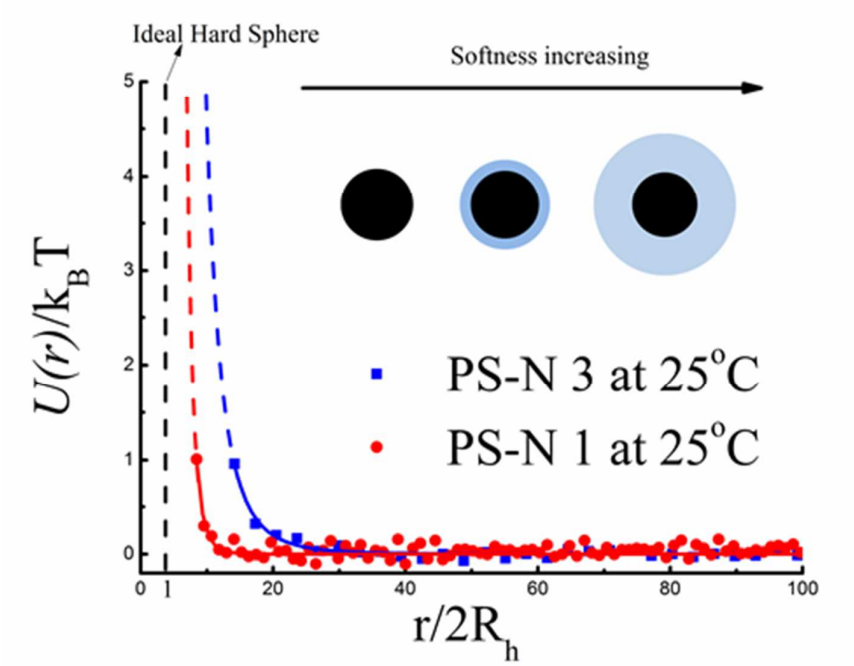

Figure 4. The interaction potential between microgel particles is plotted as a function of normalized separation, where R_h is the hydrodynamic radius of particles and r is the center-to-center distance of particles. The solid lines are the best fit using the power law interaction potential, and the dashed lines are used to guide the eye.

3.4 Shear thickening properties of PS-N microgel suspensions

Figure 5 demonstrates the steady shear viscosity of the microgel suspensions at different shear rates. In diagram (a), the results of PS-N 1 at 30°C with different effective volume fractions are shown; clearly exhibiting a shear thickening behavior. Also, as Φ_{eff} increases, the critical shear rate where the transition from shear thinning to shear thickening occurs, shifts to a lower shear rate. This occurrence agrees with

the shear thickening behavior of hard spheres. Diagram (b) demonstrates the temperature dependence of shear thickening properties for PS-N 1 microgels with fixed effective volume fraction. At 25^{o}C, no shear thickening is found within the obtainable shear rates. When the temperature increases to 28^{o}C, shear thickening starts to appear at ~3000 s^{-1}, and when it reaches 30^{o}C, very obvious shear thickening occurs at ~1000s^{-1}. Diagram (c) illustrates the shell weight fraction dependence of shear thickening with fixed effective volume fraction and temperature. For PS-N 1, apparent shear thickening properties are displayed; however, with the increase of the shell ratio, the shear thickening was never found, even at very high shear rates.

Overall, the shear thickening properties of microgel suspensions is controlled by volume fraction, temperature and shell ratio. By increasing the shell thickness and/or decreasing the temperature, the suspension can switch from shear thickening to shear thinning at high shear rates. And the critical shear rate is changed by the volume fraction like hard spheres.

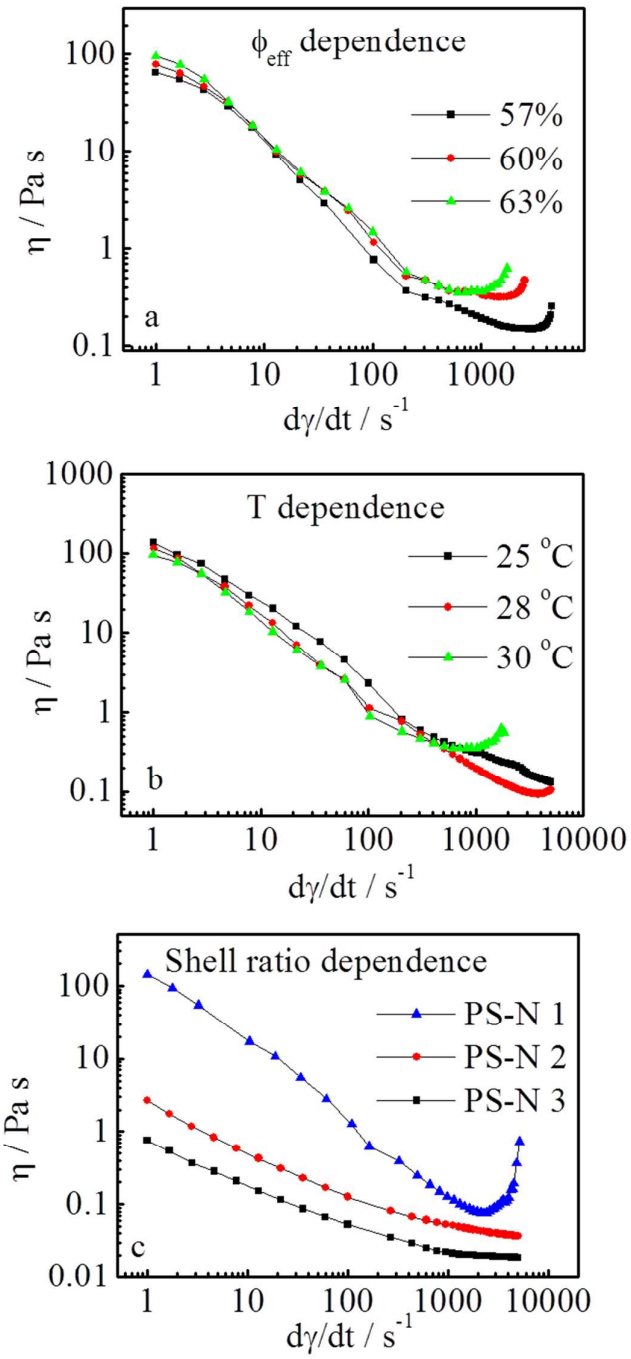

Figure 5. The steady shear rheology behavior of the core-shell particles. (a) The effective volume fraction dependence of shear thickening behavior in PS-N 1 suspension, where the temperature is fixed at 30°C (b) The effect of temperature on

shear thickening behavior in PS-N 1 suspension, where the effective volume fraction is fixed at 0.63. (c) The influence of shell ratio on shear thickening behavior, where the temperature is fixed at 28°C and the effective volume fraction is 0.67.

3.5 Influence of softness on shear thickening

Combining Table 2 and Figure 5, it is concluded that as temperature increases, the softness parameter (n) of particles increases (the softness decreases), and shear thickening behavior begins to appear and becomes more obvious. On the contrary, when shell thickness increases, the softness parameter of particles decreases, causing the suspension to change from shear thickening to shear thinning at high shear rates. Therefore the softness parameter, n, which is directly related to the inter-microgel potential in Eq. (6) and reveals the influences of both temperature and shell thickness, is actually a better parameter to measure the shear thickening property.

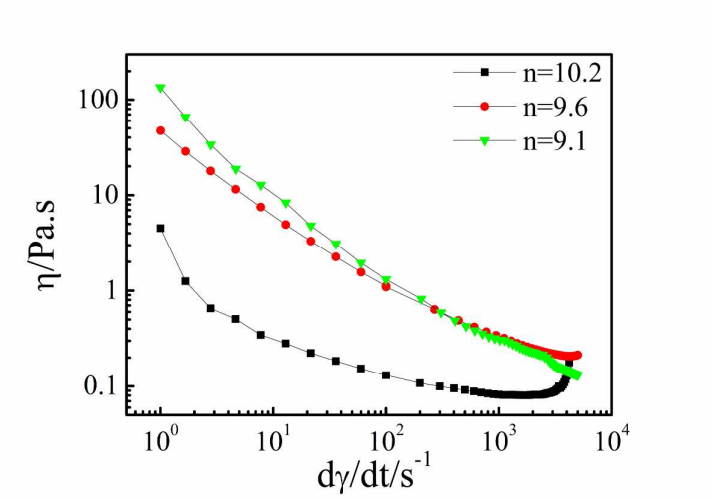

Figure 6.The steady shear rheology behavior of the PS-N microgels with different softness parameters. The triangle is the rheological behavior of PS-N 1 at 25°C, and the circles and squares are the PS-N 2 suspension at 28°C and 30°C, respectively.

In order to test and verify this assumption, the shear thickening properties of PS-N microgels with different softness parameters are plotted together. Figure 6 shows the shear behavior of three suspensions; PS-N 1 at 25^{o}C with an effective volume fraction of 105% *(n*=9.1), PS-N 2 at 28^{o}C with an effective volume fraction of 102% (*n*=9.6), and PS-N 2 at 30^{o}C with an effective volume fraction of 93% (*n*=10.2). Here, PS-N 2 at 30^{o}C, with *n*=10.2, is the "hardest" among the three samples, and displays an obvious shear thickening behavior. The softness parameter of PS-N 2 decreases with the decrease of temperature. At 28^{o}C, a very slight shear thickening behavior is only found at higher volume fractions. While PS-N 1 at 25^{o}C is the "softest" with *n*=9.1, there is no shear thickening behavior even at a high volume fraction of 105%. These results validate the notion that softness (*n*), instead of temperature or shell thickness alone, is the key factor which controls the onset of shear thickening for this core-shell PS-N system. Also, when the softness decreases (*n* becomes larger); it becomes easier for the suspension to have a shear thickening transition. Furthermore, steady shear experiments for the rest of the samples are also in agreement with the stated conclusion. When *n*<9.6, no shear thickening behavior is found within the feasible range of volume fractions and shear rates. When *n*=9.6, very slight shear thickening is observed at very high shear rates and volume fractions. For *n*≥10.2, obvious shear thickening can be easily detected. Therefore, n~9.6 may be a critical softness for PS-PNIPAM core-shell microgels to exhibit shear thickening. In summary, softness parameter *n* can be used to estimate the shear thickening behavior

of microgel suspensions.

Theoretically, the relationship between shear thickening and jamming is still under debate.[42] Currently, there are two major theories. The first theory, proposed by Bossis and Brady, states that shear thickening is caused by the formation of non-equilibrium shear induced hydroclusters, due to the short-ranged lubrication forces according to Stokesian dynamics simulations.[43–45] Wagner et al. used rheology-small angle neutron scattering (Rheo-SANS) and rheology-ultra small angle neutron scattering (Rheo-USANS) to demonstrate the existence of hydroclusters under shear conditions in reciprocal space.[46–48] They have also developed a model to predict the critical stress marking the onset of shear thickening.[4,49] Xiang Cheng et al. used fast confocal microscopy to image the hydroclusters of shear thickening colloidal suspensions in real space.[50] In our system, hydroclusters can only form when the lubrication force overcomes the repulsive force between particles and drives them together. When particle softness increases, the repulsive force between particles will increase at a given separation. Therefore, the formation of hydroclusters becomes more difficult and causes shear thickening to be suppressed in soft colloidal suspensions. Our results are not inconsistent with the hydrocluster theory.

The second theory was proposed by Holmes et al. Based on mode coupling theory (MCT), their simulation work ignored hydrodynamic interactions for dense colloids and regarded shear thickening behavior as a stress-induced transition into a jammed state[51–53]. Recently Jaeger et al also investigated the influence of jamming on shear thickening via experiments[54,55]. Their results showed that shear thickening could

be masked by a yield stress and recovered when yield stress was decreased below a threshold. However, the correlation between the experiment and parameters in this model is not clear because it requires a more careful experimental investigation of the flow behavior of very concentrated suspensions in systems of small, density-matched particles with well-controlled colloidal interactions. Our versatile core-shell particles may be suitable for such studies because they are small enough to stay in the region where Brownian motion is strong and gravity effect is weak. In addition, the interaction of the system can be conveniently tuned from hard spheres to soft microgels. These desirable features can offer a potential system to further investigate the relationship of shear thickening and jamming.

Table 3. Different parameters versus shear thickening behavior

Shear thickening (ST)				Slightly ST	No ST observed				
Sample	PS-N 1	PS-N 1	PS-N 2	PS-N 2	PS-N 1	PS-N 3	PS-N 2	PS-N 3	PS-N 3
Temperature	30°C	28°C	30°C	28°C	25°C	30°C	25°C	28°C	25°C
Softness parameter	13.1	12.6	10.2	9.6	9.1	8.5	8.3	6.7	4.9
Φ_{eff} / Φ_c	0.63/ 0.32	0.63/ 0.30	0.93/ 0.20	1.02/ 0.18	1.05/0. 30	---	---	0.67/ 0.06	---
R_{shell}/R_{core}	0.10	0.11	0.52	0.60	0.17	0.77	0.81	0.90	1.00

Table 3 lists the effects of softness, shell/core ratio and volume fraction of the hard core on the shear thickening behavior. From these results, it can easily be seen that the volume fraction of the PS hard core, Φ_c, has no direct relationship with shear thickening behavior. The shear thickening behavior is determined by the combined

effects of the core and shell, rather than the core alone. It should be noted that the starting concentrations of the shear thickening samples in this work are near or above the jamming point; therefore, they cannot flow at all before shear is applied. Under these conditions, at least the first jamming is not considered as a key point of shear thickening. In addition, the shell/core ratio, R_{shell}/R_{core}, is also excluded as a key parameter, because it neglects the influence of temperature. For PS-N 1 at 25^{o}C, the shell/core ratio is 0.17, which is much lower than 0.52 for the PS-N 2 at 30^{o}C. However, the former exhibits no shear thickening, while obvious shear thickening is observed for the latter.

Softness parameter, *n*, which combines the influence of both shell thickness and temperature, is related to the overall interaction of microgels. In Figure 4, interaction potential between particles is shown by an inverse power law potential.[56] For $r/\sigma>1$, the interaction potential of soft microgels is larger than that of corresponding hard spheres, and the larger repulsion of soft microgels would prevent the formation of hydroclusters or the stress induced jamming transition. Therefore, when *n* is too small, no shear thickening behavior is found. Deformability is another major difference between hard spheres and soft microgels. As the PS-N microgels become increasingly repulsive at room temperature with a thicker PNIPAM shell, it also acquires a greater chance of being deformed at higher shear rates. Whereas for $r/\sigma<1$, the interaction potential of a softer particle is smaller, which means that softer microgels undergo more interpenetration and deformation. AFM experiments showed that softer microgels have a lower particle modulus[57]. Rheo-SANS data also revealed that the

anisotropy in particles exists when the suspension is under shear (see Supporting Information). The deformation of particles can also influence the formation of hydroclusters or the stress induced jamming transition. However, further investigations are needed in order to explore the relationship between hydroclusters or stress induced jamming structures and various model parameters, such as the amplitude of thermal fluctuation, soft interaction potential and hydrodynamic interaction.

4 Conclusions

The shear thickening properties of a series of PS-N core-shell microgels with different shell thicknesses were studied at various temperatures and concentrations. The structure and effective volume fraction of the suspensions are characterized by TEM, DLS and viscometry. Rheological experiments showed that a softness parameter, n, derived from the Zwanzig and Mountain equation, could describe the combined influences of temperature and shell thickness. The softness of microgels increased with decreasing the temperature, but at the same time increased with increasing shell thickness. Confocal microscopy results indicated that the repulsive force between particles increased with the increase of softness. On the other hand, as temperature increased or shell thickness decreased, the suspension changed from shear thinning to shear thickening at high shear rates. Further experiments suggested that the softness parameter, n, can be used to semi-quantitatively estimate the shear thickening behavior of microgel suspensions. For relatively soft particles (n is small), no shear

thickening behavior was observed within the feasible range of volume fractions and shear rates. For harder particles (*n* is relatively larger), shear thickening can be easily observed. Furthermore, a critical softness (*n*=9.6) for PS-PNIPAM core-shell microgels to exhibit shear thickening was determined. The main reason for the suppression of shear thickening in soft microgels suspension may be divided into two parts; a larger repulsion and possible deformation of the microgel network.

Acknowledgements

The financial support from the National Basic Research Program of China (973 Program, 2012CB821500), and National Natural Scientific Foundation of China (No. 21174152) is gratefully acknowledged. Javoris Hollingsworth was supported by the National Science Foundation (OISE-1159189).

References

1. Y. S. Lee, E. D. Wetzel, and N. J. Wagner, *J. Mater. Sci.*, 2003, **38**, 2825 – 2833.
2. N. J. Wagner and J. F. Brady, *Phys. Today*, 2009, 27–32.
3. D. P. Kalman, R. L. Merrill, N. J. Wagner, and E. D. Wetzel, *ACS Appl. Mater. Interfaces*, 2009, **1**, 2602–2612.
4. B. Maranzano and N. Wagner, *J. Chem. Phys.*, 2001, **114**, 10514–10527.
5. B. Maranzano and N. Wagner, *J. Rheol.*, 2001, **45**, 1205–1222.
6. P. D'Haene, J. Mewis, and G. G. Fuller, *J. Colloid Interface Sci.*, 1993, **156**, 350–358.
7. W. H. Boersma, *J. Rheol.*, 1991, **35**, 1093–1120.

8. H. Senff and W. Richtering, *J. Chem. Phys.*, 1999, **111**, 1705–1711.

9. H. Senff, W. Richtering, C. Norhausen, A. Weiss, and M. Ballauff, *Langmuir*, 1999, **15**, 102–106.

10. M. Siebenbürger, M. Fuchs, and M. Ballauff, *Soft Matter*, 2012, **8**, 4014–4024.

11. R. Zwanzig and R. Mountain, *J. Chem. Phys.*, 1965, **43**, 4464–4471.

12. S. E. Paulin, B. J. Ackerson, and M. S. Wolfe, *J. Colloid Interface Sci.*, 1996, **178**, 251–262.

13. N. Koumakis, A. Pamvouxoglou, A. S. Poulos, and G. Petekidis, *Soft Matter*, 2012, **8**, 4271–4284.

14. J. Vermant and M. J. Solomon, *J. Phys. Condens. Matter*, 2005, **17**, R187–R216.

15. J. Kim and M. Ballauff, *Colloid Polym. Sci.*, 1999, **277**, 1210–1214.

16. N. Dingenouts, S. Seelenmeyer, I. Deike, S. Rosenfeldt, M. Ballauff, P. Lindner, and T. Narayanan, *Phys. Chem. Chem. Phys.*, 2001, **3**, 1169–1174.

17. H. Cui, T. Hodgdon, E. Kaler, and L. Abezgauz, *Soft Matter*, 2007, **3**, 945–955.

18. S. Seelenmeyer, I. Deike, S. Rosenfeldt, C. Norhausen, N. Dingenouts, M. Ballauff, T. Narayanan, and P. Lindner, *J. Chem. Phys.*, 2001, **114**, 10471–10478.

19. W. Poon, E. Weeks, and C. Royall, *Soft Matter*, 2012, **8**, 21–30.

20. G. Batchelor, *J. Fluid Mech.*, 1977, **83**, 97–117.

21. D. P. Kalman, B. A. Rosen, N. J. Wagner, A. Co, G. L. Leal, R. H. Colby, and A. J. Giacomin, in *AIP Conference Proceedings*, AIP, 2008, vol. 1027, pp. 1408–1410.

22. A. Le Grand and G. Petekidis, *Rheol. Acta*, 2008, **47**, 579–590.

23. J. Mewis and G. Biebaut, *J. Rheol.*, 2001, **45**, 799–813.

24. V. Gopalakrishnan and C. F. Zukoski, *J. Rheol.*, 2004, **48**, 1321–1344.

25. J. Mewis and N. J. Wagner, *Colloidal Suspension Rheology*, Cambridge University Press, Cambridge, 2011.

26. S. Hirotsu, Y. Hirokawa, and T. Tanaka, *J. Chem. Phys.*, 1987, **87**, 1392–1395.

27. M. Shibayama, T. Tanaka, and C. C. Han, *J. Chem. Phys.*, 1992, **97**, 6829–6841.

28. H. Cheng, L. Shen, and C. Wu, *Macromolecules*, 2006, **39**, 2325–2329.

29. L. A. Lyon and M. J. Serpe, *Hydrogel Micro and Nanoparticles*, Wiley-VCH Verlag GmbH & Co. KGaA, Weinheim, Germany, 2012.

30. P. Kujawa and F. M. Winnik, *Macromolecules*, 2001, **34**, 4130–4135.

31. J. J. Crassous, M. Siebenbürger, M. Ballauff, M. Drechsler, O. Henrich, and M. Fuchs, *J. Chem. Phys.*, 2006, **125**, 204906.

32. J. Wu, B. Zhou, and Z. Hu, *Phys. Rev. Lett.*, 2003, **90**, 048304.

33. A. Zaccone, J. Crassous, B. Béri, and M. Ballauff, *Phys. Rev. Lett.*, 2011, **107**, 168303.

34. N. Dingenouts, C. Norhausen, and M. Ballauff, *Macromolecules*, 1998, **31**, 8912–8917.

35. N. J. Wagner, *J. Colloid Interface Sci.*, 1993, **161**, 169–181.

36. G. Bryant, S. Williams, L. Qian, and I. Snook, *Phys. Rev. E*, 2002, **66**, 060501.

37. C. Royall, W. Poon, and E. Weeks, *Soft Matter*, 2013, **9**, 17–27.

38. J. Ferguson and Z. Kemblowski, *Applied Fluid Rheology*, Elsevier Applied Science, 1991.

39. J. K. Cho, Z. Meng, L. A. Lyon, and V. Breedveld, *Soft Matter*, 2009, **5**, 3599–3602.

40. H.-J. Wu, T. O. Pangburn, R. E. Beckham, and M. a Bevan, *Langmuir*, 2005, **21**, 9879–9888.

41. Y. Han and D. Grier, *Phys. Rev. Lett.*, 2003, **91**, 038302.

42. E. Bertrand, J. Bibette, and V. Schmitt, *Phys. Rev. E*, 2002, **66**, 060401.

43. J. F. Brady and G. Bosis, *J. Fluid Mech.*, 1985, **155**, 105–129.

44. T. N. Phung, J. F. Brady, and Georges Bossis, *J. Fluid Mech.*, 1996, **313**, 181–207.

45. G. Bossis and J. F. Brady, *J. Chem. Phys.*, 1989, **91**, 1866–1874.

46. D. P. Kalman and N. J. Wagner, *Rheol. Acta*, 2009, **48**, 897–908.

47. Y. Lee and N. Wagner, *Ind. Eng. Chem. Res.*, 2006, **45**, 7015–7024.

48. B. J. Maranzano and N. J. Wagner, *J. Chem. Phys.*, 2002, **117**, 10291–10302.

49. L.-N. Krishnamurthy, N. J. Wagner, and J. Mewis, *J. Rheol.*, 2005, **49**, 1347–1360.

50. X. Cheng, J. McCoy, J. Israelachvili, and I. Cohen, *Science*, 2011, **333**, 1276–1279.

51. C. B. Holmes, M. Fuchs, and M. E. Cates, *Europhys. Lett.*, 2003, **63**, 240–246.

52. C. Holmes, M. Cates, M. Fuchs, and P. Sollich, *J. Rheol.*, 2005, **49**, 237–269.

53. E. Lerner, G. Düring, and M. Wyart, *Proc. Natl. Acad. Sci. U. S. A.*, 2012, **109**, 4798–4803.

54. E. Brown, N. A. Forman, C. S. Orellana, H. Zhang, B. W. Maynor, D. E. Betts, J. M. DeSimone, and H. M. Jaeger, *Nat. Mater.*, 2010, **9**, 220–224.

55. E. Brown and H. M. Jaeger, *J. Rheol.*, 2012, **56**, 875–912.

56. D. Heyes and A. Brańka, *Soft Matter*, 2009, **5**, 2681–2685.

57. S. M. Hashmi and E. R. Dufresne, *Soft Matter*, 2009, **5**, 3682–3688.

Table of Contents Entry

Effects of particle softness on shear thickening of microgel suspensions

*Zhi Zhou,[1, 2] Javoris V. Hollingsworth,[1] Song Hong,[3] Guangmin Wei,[1] Yu Shi,[1] Xi Lu,[1] He Cheng,[4,] * Charles C. Han[1,]**